Eulerian simulation of coaxial injection using an interfacial surface density balance equation

Stéphane Jay[†], François Lacas[‡], and Sébastien Candel[*]
[†] Institut Français du Pétrole
3,4 avenue de Bois Préau
92500 Rueil-Malmaison
[‡],[*] Laboratoire EM2C, CNRS UPR 288, Ecole Centrale Paris
Grande Voie des Vignes
92295 Chatenay-Malabry Cedex, France
[*] and Institut Universitaire de France
[†] Stephane.Jay@ifp.fr,[‡] Francois.Lacas@em2c.ecp.fr, [*] Sebastien.Candel@em2c.ecp.fr

Abstract

The spray formed by a coaxial injector fed with water and air is modeled and simulated in this paper. The purpose is to perform global validations of the flow structure using an interfacial surface density balance equation. The field equations are described in the context of an homogeneous flow code and special attention is paid to the modeling of the drift between the two phases. An additional balance equation for the interfacial surface density represents the instability development, its saturation and subsequent atomization. The source terms accounting for these various mechanisms are modeled. Numerical calculations are then carried out and results are compared with data from two generic experiments. The computed intact core length is in good agreement with measurements. A semi-empirical method is proposed to deduce interfacial surface density profiles from liquid droplets size and velocity measurements. Orders of magnitudes are well reproduced by the model. The spray expansion at a few injector diameters is reproduced and the computed interfacial surface density levels are of the same order of magnitude as those obtained from measurements. The largest differences are observed within a few injector diameters from the injection plane in the dense spray region where measurement methods are less well suited.

1. Introduction

Coaxial injectors are used in a broad range of industrial applications where high mass flow rates are required. In rocket engines a large number of units in "showerhead" arrangements feed the chamber. In most cases one of the reactants (fuel or oxidizer) is injected in a liquid form while in some cases the two propellants are liquid. The efficiency of coaxial injectors mainly depends on the quality of the liquid jet break up and subsequent atomization. Recent experiments on coaxial injectors [1-5] have focused on these two processes and on their effects on the flame structure. In rocket engine injectors the liquid is delivered at relatively low speed (a few m s^{-1}) and is surrounded by an annular stream of gas at high speed (a few hundred m s^{-1}). A perturbation at the liquid gas interface is rapidly amplified by the velocity differential and the interfacial surface area is increased. At a distance from the injection plan, nonlinear mechanisms take over and the growth rate is saturated. The interface perturbations form wave-like structures which propagate at a velocity U_c defined by a weighted average of the velocities

of the gaseous and liquid phases. The numerical modeling of these processes is a difficult task which is here approached in an Eulerian framework. The analysis concerns the two-phase flow formed by a coaxial injector fed by water and air and operating at ambiant pressure. A transport equation for the density of liquid interface is exploited to represent the jet break-up, subsequent atomization and evolution of the liquid surface area. This equation and associated submodels are incorporated in the Kiva3 code modified to account for the velocity differential in a formulation based on a diffusion (or mixture) model. This description reduces the two-fluid Eulerian formalism to a homogeneous model with a drift velocity (see for example Ishii [6]). The drift velocity is deduced from a standard gradient model. The various elements of this model are first described. Numerical calculations are then carried out and results are compared with data from two generic experiments.

2. Field equations

The balance of mass for the homogeneous two-phase mixture requires a transport equation for the gaseous phase mass concentration ρ_g and a transport equation for the liquid phase mass concentration ρ_l. The average density of the mixture is $\rho_m = \overline{\rho} = \rho_g + \rho_l$. The transport equation of the gaseous phase mass concentration has the form

$$\frac{\partial \rho_g}{\partial t} + \boldsymbol{\nabla} \cdot (\rho_g \mathbf{v}_m) = \boldsymbol{\nabla} \cdot \rho_m \mathbf{V}_g^D \tag{1}$$

The diffusion velocity of the gaseous phase $\mathbf{V}_g^D$ is given by relation (2)

$$\rho_m \mathbf{V}_g^D = \rho_m D_g \boldsymbol{\nabla} \left(\frac{\rho_g}{\rho_m} \right) + \rho_g \mathbf{V}_{gm} \tag{2}$$

Coefficient D_g is deduced from the turbulent viscosity and a Schmidt number $\rho_m D_g = \mu_t / Sc$ with $\mu_t = \mu_m + C_\mu k^2/\epsilon$ where the dynamic viscosity of the homogeneous flow is a function of the liquid volume fraction. The last term $\rho_g \mathbf{V}_{gm}$ in expression (2) describes transfer processes due to drift between the gas and liquid phases.

The liquid phase concentration satisfies a balance equation with an additional source term representing the drift between the two phases

$$\frac{\partial \rho_l}{\partial t} + \boldsymbol{\nabla} \cdot (\rho_l \mathbf{v}_m) = \boldsymbol{\nabla} \cdot \rho_m \mathbf{V}_l^D \tag{3}$$

The diffusion velocity is given by an expression similar to that used for the gas

$$\rho_m \mathbf{V}_l^D = \rho_m D_l \boldsymbol{\nabla} \left(\frac{\rho_l}{\rho_m} \right) + \rho_l \mathbf{V}_{lm} \tag{4}$$

The last term $\rho_l \mathbf{V}_{lm}$ in this expression describes transfer due to drift between phases. Determination of the diffusion velocities $\mathbf{V}_g^D$ and $\mathbf{V}_l^D$ requires a closure for the drift velocities $\mathbf{V}_{gm} = \mathbf{v}_g - \mathbf{v}_m = (\rho_l/\rho_m)\mathbf{v}_r$ and $\mathbf{V}_{lm} = \mathbf{v}_l - \mathbf{v}_m = -(\rho_g/\rho_m)\mathbf{v}_r$ where the local velocity differential $\mathbf{v}_r = |\mathbf{v}_r|\mathbf{b}$ is expressed in terms of its magnitude $|\mathbf{v}_r|$ and its direction $\mathbf{b}$. The magnitude is modeled in terms of the volume fraction gradient

$$|\mathbf{v}_r| = D_\alpha \frac{1}{\alpha_l(1-\alpha_l)} |\boldsymbol{\nabla} \alpha_l|$$

In this expression α_l is defined as $\alpha_l = \rho_l/\langle\rho_l\rangle$ where $\langle\rho_l\rangle$ is the average liquid density on the liquid phase ($\langle\rho_l\rangle$ = 1000 kg m^{-3}). The coefficient D_α is given in terms of the initial velocity differential $\Delta U = U_g - U_l$. The region in which D_α is calculated is such that $\alpha_l < (\alpha_l)_c$ where $(\alpha_l)_c$ is a maximum volume fraction which defines the spray boundary ($(\alpha_l)_c$ = 10^{-2} in the simulations).

$$D_\alpha = \frac{1}{2}\frac{(U_l - U_g)\delta_g}{\ln \alpha_l} \tag{5}$$

The thickness of the shear layer δ_g is estimated from the local conditions in the gas flow $\delta_g = (D_{go} - D_{gi})/\mathrm{Re}_g^{1/2}$. In the initial region corresponding to the injector nearfield where the two phases are essentially separated, D_α is calculated with the limit liquid volume fraction $(\alpha_l)_c$=10^{-2}.

The direction of the relative velocity $\mathbf{b}$ near the injection plane is supposed to be the same as the direction of the liquid or the gas flow : $\mathbf{b} = \mathbf{v}_r/|\mathbf{v}_r| = \mathbf{v}_m/|\mathbf{v}_m|$. By summing equation (1) and equation (3) one obtains the mixture balance of mass

$$\frac{\partial \rho_m}{\partial t} + \boldsymbol{\nabla}\cdot(\rho_m \mathbf{v}_m) = 0 \tag{6}$$

The conservation of momentum of the homogeneous mixture is given by

$$\frac{\partial \rho_m \mathbf{v}_m}{\partial t} + \boldsymbol{\nabla}\cdot(\rho_m \mathbf{v}_m \mathbf{v}_m) = -\boldsymbol{\nabla} p_m + \boldsymbol{\nabla}\cdot\overline{\tau}^t + \boldsymbol{\nabla}\cdot\overline{\tau}^l - \boldsymbol{\nabla}\cdot\sum_k \alpha_k\langle\rho_k\rangle V_{km}^2 \tag{7}$$

The viscous stress tensor $\overline{\tau}^l$ is represented with a Newtonian model while the turbulent stress tensor is expressed in terms of a turbulent viscosity (k,ϵ) model. The last term in relation (7) describes momentum transfer due to the drift between phases. The previous closure relations are used to model $\mathbf{V}_{gm}$ and $\mathbf{V}_{lm}$.

The previous set of equations describes the two-phase flow of a homogeneous mixture without mass transfer. To complete this description of the spray an additional equation is used for the interfacial surface density between liquid and gaseous phases. This quantity designated as Σ_i defines the amount of surface area per unit volume of the mixture. It gives information on the liquid phase structure.

3. Interfacial area density equation

A balance equation may be derived for the liquid/gas interface density Σ_i which accounts for the mechanisms controlling the development of the droplet spray. This equation takes the general form

$$\frac{\partial \Sigma_i}{\partial t} + \mathbf{u}\cdot\boldsymbol{\nabla}\Sigma_i = D + P_1 E_1 + P_2 + P_3 - D_2 \tag{8}$$

where D, P_1E_1, P_2, P_3, D_2 respectively describe turbulent diffusion of interfacial surface area, production P_1 by shear instability and its saturation (E_1), production by secondary atomisation (P_3), production by microscale turbulence (P_2), saturation of secondary atomisation when the critical Weber number is reached (D_2). Expressions of source terms P_2 and D_2 are those derived by Borghi and Vallet [7]. Explicit forms of source terms P_1E_1 and P_3 are detailed in what follows.

Special attention is paid to the evolution of interfacial surface density in the primary break-up zone and to the modeling of source term $P_1 E_1$. The instability in this region may be analyzed by assuming that a linear velocity profile is established in the gas phase near the liquid interface. The thickness of this shear layer is δ_g. A temporal instability analysis of the type initially developed by Rayleigh indicates that the wavelength of the most amplified disturbances λ_{max} depends on the shear layer thickness δ_g in the gas stream ($\lambda_{max} \simeq \delta_g(\rho_l/\rho_g)^{1/2}$). The growth rate can be written $\alpha = b_1(\rho_l/\rho_g)^{1/2}|U_g - U_l|\kappa_{max}$ where κ_{max} is the most amplified wave number ($\kappa_{max} = 2\pi/\lambda_{max}$). This destabilization process induces an increase of the interfacial surface density Σ_i. This mechanism is effective close to the injector outlet. Further downstream the primary instability is saturated by nonlinear processes and the interfacial area levels-off. This may be modeled by reducing the growth rate as the surface density increases. A non linear equation may be used to represent the initial growth and later saturation of the interfacial surface area

$$\frac{d\Sigma_i}{dt} = \alpha(1 - \eta_i^2 {\Sigma_i}^2)^{1/2} \Sigma_i h(1 - \eta_i \Sigma_i) \tag{9}$$

In this expression h, the Heaviside function ($h(x) = 1$ if $x \geq 0$, $h(x) = 0$ if $x < 0$), brings the growth rate to zero when Σ_i has reached a value of $1/\eta_i$. The nonlinear saturation parameter η_i may be estimated from the evolution of Σ_i as a function of time. One finds that $\eta_i \simeq C \exp(-B_1\sqrt{\rho_g/\rho_l}(D_l/\delta_g)f(J))$ where J is the gas to liquid momentum flux ratio $J = \rho_g U_g^2/\rho_l U_l^2$ and $f(J)$ defines the evolution of the liquid core length. One can use experimental or semi-empirical results to express the relation between the momentum flux ratio J and the break-up length.

The product of the growth rate α by the interfacial surface density defines term P_1 of equation (8) : $P_1 = \alpha\Sigma_i$. The growth rate in this expression is given by

$$\alpha = b_1 \frac{\rho_g}{\rho_l} \frac{|\mathbf{v}_r|}{\delta_g} \tag{10}$$

where the relative velocity $|\mathbf{v}_r|$ between the two phases is calculated according to the rules given in the previous section and modeled by relation (5). The saturation term in equation (9) constitutes the equilibrium term E_1=$(1-\eta_i^2{\Sigma_i}^2)^{1/2}h(1-\eta_i\Sigma_i)$. The computation of the source term P_1E_1 of interfacial instability uses the parameters presented in table 1.

Shear layer thickness	$\mathrm{Re}_g = \frac{\langle\rho_g\rangle_g \|\mathbf{v}_g\|(D_{go}-D_{gi})}{\mu_g}$	$\delta_g = \frac{D_{go}-D_{gi}}{\mathrm{Re}_g^{1/2}}$
Break-up length	$L_{bu} = C_{bu} f(J)$	$J = \frac{\rho_g U_g^2}{\rho_l U_l^2}$
Saturation parameter		$\eta_i = \frac{1}{2}\exp\left[-B_1\sqrt{\frac{\rho_g}{\rho_l}}\frac{D_l}{\delta_g}f(J)\right]$

Table 1: Parameters used for the computation of the source term P_1E_1 of interfacial area.

The computation of secondary atomisation mechanisms (source term P_3) uses an average local Weber number $\mathrm{We} = (\langle\rho_g\rangle_g|\mathbf{v}_r|^2 d_{32})/\sigma$ and an expression for the maximum droplet diameter $d_{max} = (We_c\sigma/\rho_m)^{3/5}\epsilon^{-2/5}$. An equivalent Sauter mean diameter without secondary atomisation is estimated from the liquid / gas interfacial density $d_{32} = 6\alpha_l/\Sigma_i$. The secondary

atomisation break-up time τ_{bu} is based on this last diameter d_{32} and it is obtained from expression (11) given by Amsden & O'Rourke [9].

$$\tau_{bu} = C_\tau \sqrt{\frac{\langle \rho_l \rangle_l d_{32}^3}{8\sigma}} \tag{11}$$

This last expression corresponds to the Taylor Analogy Break-Up model. Finally, the formulation of the transport equation for the interfacial area including diffusion D, production by interfacial instability $P_1 E_1$ and production by secondary break-up is the following

$$\begin{aligned} \frac{\partial \widetilde{\Sigma_i}}{\partial t} + \boldsymbol{\nabla} \cdot (\mathbf{v}_m \widetilde{\Sigma_i}) &= \boldsymbol{\nabla} \cdot \left(D_{\Sigma_i} \boldsymbol{\nabla} \widetilde{\Sigma_i} \right) \\ &+ \alpha \widetilde{\Sigma_i} \left(1 - \left(\eta_i \widetilde{\Sigma_i} \right)^2 \right)^{1/2} h(1 - \eta_i \widetilde{\Sigma_i}) \\ &+ h(d_{32} - d_{max}) \frac{\widetilde{\Sigma_i}}{\tau_{bu}} \end{aligned} \tag{12}$$

Systematic calculations have been carried out with this model and with the alternate equation of Borghi and Vallet. In particular, the model equation (8) is tested with two combinations of source terms. The first (IM_1) includes D,$P_1 E_1$,P_3. The second (IM_2) uses D,P_2,D_2.

Conditions used in the calculations are those corresponding to fiber and superpulsating modes of operation of the liquid / gas coaxial injector. The simulations are carried out for a coaxial injection unit device used by Leroux [3] and by Werquin [10]. Liquid core length evolution is estimated from the calculated interfacial surface density field and is compared with measurements of Leroux based on backlighting [3] and of Werquin relying on laser induced fluorescence [10].

Geometrical features			
Liquid jet diameter	D_l	0.4	mm
Internal gaseous diameter	D_{gi}	1.0	mm
External gaseous diameter	D_{go}	3.5	mm
Injector lip thickness	$\epsilon = (D_{gi} - D_l)/2$	0.3	mm
Physical parameters			
Liquid surface tension	σ	72.8 10^{-3}	Nm^{-1}
Injection parameters			
Gas injection velocity	U_g	133	ms^{-1}
Liquid injection velocity	U_l	1-2.5	ms^{-1}
Injection momentum flux ratio	$J = \rho_g U_g^2 / \rho_l U_l^2$	3.3-20.5	-

Table 2: Coaxial injector geometry and operating parameters.

In the injector far field, comparisons are made between the droplet size measurements of Leroux [3] and the equivalent Sauter mean diameter deduced from the calculated liquid surface density and volume fraction.

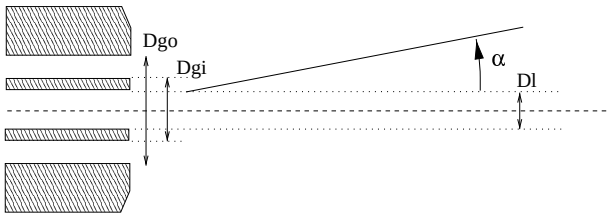

Figure 1: Scheme of a coaxial injector.

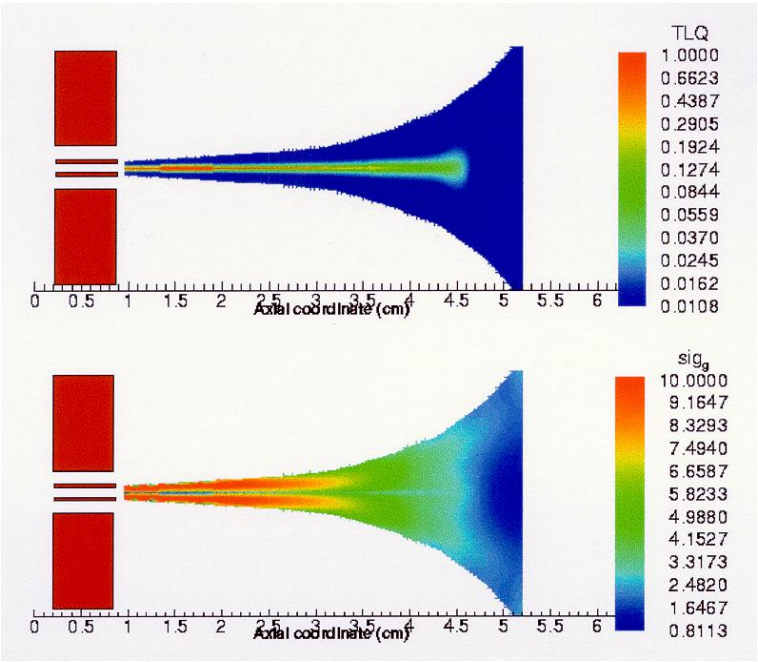

Figure 2: Liquid volume fraction α_l (top) and interfacial surface density Σ_i in cm^{-1} (bottom) - U_l=2.5 ms^{-1} U_g=133 ms $^{-1}$ J = 20.5.

4. Structure of the dense spray region

When the spray structure is dispersed, which is the case for membrane or superpulsating atomisation type, the radial distribution of liquid spreads in the radial direction at a few injector diameters from the injection plan. In these cases, the intact liquid region (the liquid core) is limited in space. The break-up length L_{bu} defines the size of this region. Numerical simulations are used to calculate the evolution of this quantity which is deduced from the interfacial surface density. Recent studies of coaxial injectors indicate that L_{bu} is mainly controlled by the gas to liquid momentum flux ratio.

The coaxial injector shown in figure 1 is fed with water and air at ambient pressure and temperature. The velocity of the air jet is held constant at U_g=133ms^{-1} to ensure a constant turbulence level in the gaseous flow (Re$_g$ $\simeq$ 21000). The liquid velocity U_l varies between 1 and 2.5 ms^{-1} (see table 2).

The interfacial surface density and the liquid volume fraction calculated fields are dis-

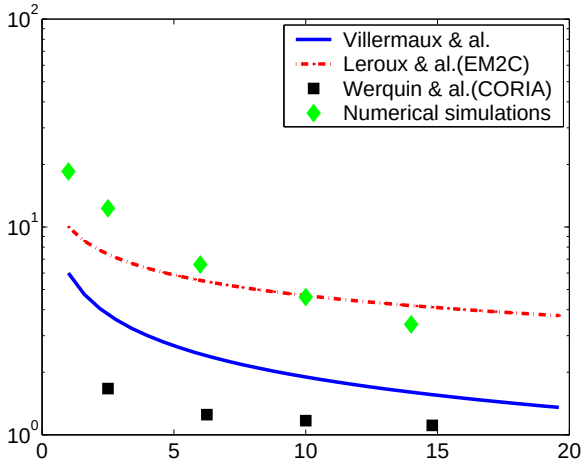

◇) is compared to break-up length correlations deduced from experimental investigations of Leroux (2002) represented by a dashed line, Werquin [10] represented by (□) symbols or semi-empirical analysis of Ref. [8] represented by a solid line.

played in figure 2. The axial position of the maximum in interfacial surface density is used to determine the liquid core length. This determination of the core length is chosen because it is convenient but somewhat arbitrary. The calculated evolution is displayed in figure together with experimental correlations and the semi-empirical rule of Ref. [8].

The global evolution of the break-up length obtained numerically agrees to a certain extent with the experimental correlation proposed in Ref. [3] and the theroretical correlation of Ref. [8]. Numerical estimates are centered on the correlation of Leroux [3] plotted in dashed line. For a momentum flux ratio under 5, the computations overestimate the break-up length. For momentum flux ratios J between 5 and 15, the calculated values agree with the experimental correlation. This was to be expected because the liquid core expression in terms of the momentum flux ratio is used to determine the saturation parameter η_i.

Numerical results are also compared to measurements given in Ref. [10] and represented by (□) symbols. The liquid core size determined from laser induced fluorescence images is consistently lower than values obtained by other methods. In these experiments, the momentum flux ratio J and the injection Weber number We are varied to study the evolution of the liquid core length. The results obtained show a dependency of the liquid core with $J^{-1/2}$ when We is kept constant. For the purpose of comparisons, we have chosen measurements at We=1225 which are closest to our simulation conditions. Moreover the geometrical configuration is not exactly the same as the simulated one.

The evolution of length of the liquid core is reproduced to some extent by the model. Nevertheless the dependency on the J number does not exactly match that found in experiments but the data is also widely scattered. It would be possible to obtain a better agreement between experimental data and numerical estimates but this would not be useful at this point since the size of liquid core is not a well defined quantity and its values depend on the measurement technique. The definition adopted for its numerical estimation is also somewhat arbitrary.

5. Influence of injection on the diluted spray region

The balance equation for the interfacial surface density describes processes of primary break-up and atomization which yield the far field spray distribution. It is interesting to examine the evolution of interfacial surface area from the near field to the far field. This quantity is usually not determined experimentally. It is however possible to deduce an effective surface density from distributions of droplet sizes and liquid phase velocities. Consider an axial section located at a distance from the injector where the spray may be considered to be uniform. In this section the spray cross section is $A_s = \pi R_s^2$. The droplets have a mean Sauter diameter d_{32} and their mean velocity is $\overline{u}_l$. One may deduce the droplet density from

$$n = \frac{\dot{m}}{\rho_l \overline{u}_l A_s \frac{1}{6}\pi d_{32}^3} \tag{13}$$

where $\dot{m}_l$ is the injected liquid mass flow rate. The spray radius R_s can be calculated by using a correlation (14) established in Ref. [3] for the spray half-angle

$$\tan\frac{\alpha}{2} = \frac{0.72\sqrt{J}(1-0.1\sqrt{J})}{0.06J+\sqrt{J}+1} \tag{14}$$

The spray radius R_s at an axial position z is $R_s = R_l + z\tan\alpha/2$ where R_l is the liquid jet radius in the injection plan (see figure 1). The liquid volume fraction is simply given by $\alpha_l = (1/6)\pi d_l^3 n$ and the interfacial density Σ_i for the dispersed spray is computed by equation $\Sigma_i = 6\alpha_l/d_l$.

Radial profiles of computed interfacial surface density are displayed in figure 4 at z=4D_{go} (solid line) and z=12 D_{go} (dashed line). Direct comparisons are made with the values deduced from experiments by the method exposed above. The experimental values at z=4D_{go} are represented by (+) symbols. Those at z=12 D_{go} are represented by (○) symbols. The order of magnitude of the measured interfacial density are close to those deduced from experiments. The spray expansion is also reproduced. The interfacial area density increases from the jet axis towards the periphery of the spray. The main differences are observed for the values calculated on the injector axis.

Combined with the mean liquid volume fraction $\tilde{\alpha}_l$, the interfacial density provides an estimate of the equivalent Sauter mean diameter ($d_{32} = 6\tilde{\alpha}_l/\tilde{\Sigma}_i$). Results obtained with source terms representing the shear layer instability P_1E_1 and secondary atomisation P_3 in equation 8 are compared in Figure 5 with estimates obtained by considering only a far field equilibrium P_2, D_2 (see Ref. [7]). Radial evolutions are shown in Figure 5 at different axial positions (here D_{go} is the injector outer diameter). The order of magnitude of the droplet sizes calculated are in agreement with those measured in Ref. [3] with Phase Doppler Anemometry (PDPA) technique. Calculations predict that the largest droplets are close to the axis whereas the smallest droplets are located in the periphery of the spray. Nevertheless, in the near field (z=4D_{go}), values calculated on the injector axis with the interfacial instability development are higher than those measured in Ref. [3] and than those predicted by the far field equilibrium. Shadowgraph images of the spray show that large liquid structures are present in this region at the end of the liquid core. These structures are not accurately measured by PDA and this probably explains the differences between the simulations and the experimental data.

The spray also extends over a narrower domain in the simulations than in the experiments but one should remember that a lower validation rate is obtained in the measurements in the periphery of the spray and as a consequence the data in this region is less reliable. The model-

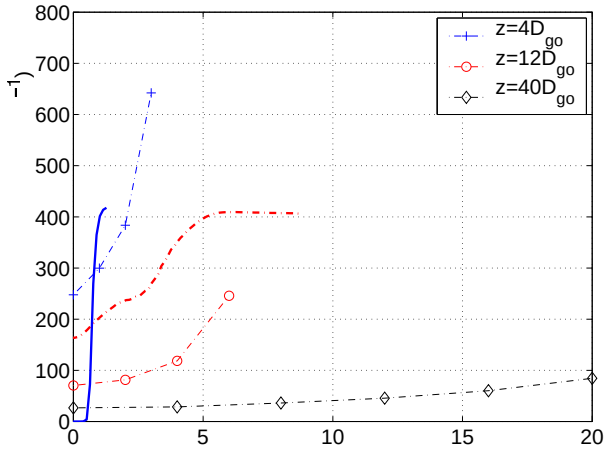

Σ_i deduced from measurements at axial position z=4D_{go} (+), z=12D_{go} (○), z = 40 D_{go} (◇). These values use experimental results of Ref. [3] for the droplet axial velocities u_l and Sauter mean diameter d_l. The injection velocities are U_l=1 ms^{-1} and U_g=133ms^{-1} which corresponds to a momentum flux ratio J=20.5. The solid line corresponds to numerical estimates at z=4D_{go} while the dashed doted line corresponds to z=12 D_{go}.

ing of the turbulent dispersion of the liquid phase also needs improvements and it is possible that the simulations underestimate the spray expansion because the liquid / gas turbulent interactions level is not sufficiently well calculated.

6. Conclusions

A model including primary and secondary break-up effects is investigated in the context of coaxial injection. It relies on a description of the drift between the two phases in an Eulerian framework and on a balance equation for interfacial surface density. The modeling is tested in two generic cases which provide basic elements for the spray description such as the primary break-up characteristic length or interfacial density levels in the diluted spray region. The intact liquid core length dependence on the momentum flux ratio is well reproduced by the model. The computed interfacial surface density levels are of the same order of magnitude as those obtained from measurements. The largest differences are observed on the axis within a few injector diameters from the injection section where the spray is dense. In the diluted region, the description of the flow certainly misses a more reliable turbulence model involving droplet/gas interactions which would improve the spray expansion modeling. The balance equation IM_1 including primary break-up effects and secondary atomization seems to better describe the droplet mean diameter in the far field. Further work is needed to test the validity of the model in other injection configurations.

Acknowledgments

This work was financially supported by SNECMA and CNRS in the framework of the

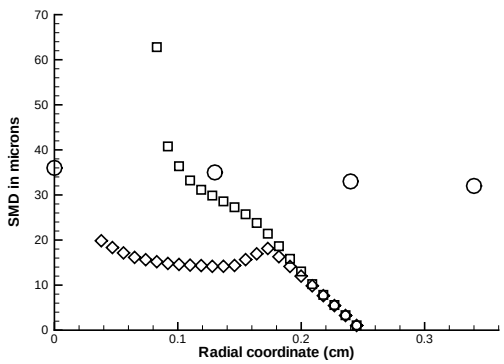

z=4D_{go}, U_l=2.5 ms^{-1}, U_g=133 ms^{-1}

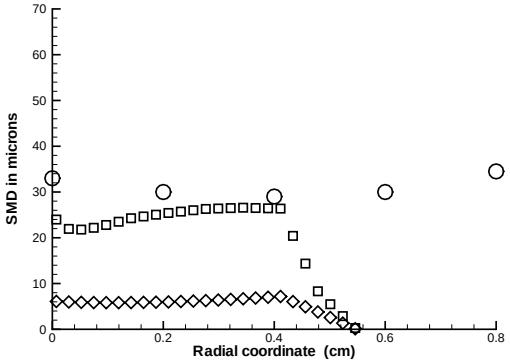

z=12D_{go}, U_l=2.5 ms^{-1}, U_g=133 ms^{-1}

Figure 5: Comparison of measured and calculated Sauter mean diameter (μm) - ◯ Experimental data (Leroux), □ IM_1 instability model & secondary atomization (D,P_1E_1,P_3), ◇ IM_2 far field equilibrium model (D,P_2,D_2).

GDR Combustion in Liquid Rocket Engines. Special thanks are addressed to IDRIS which provided the computational resources used in this project.

References

[1] Juniper M, Tripathi A, Scouflaire P, Rolon C and Candel S 2001 *Proceedings of the Combustion Institute* **28** 1103

[2] Rehab H, Villermaux E and Hopfinger E J 1997 *Journal of Fluid Mechanics* **345** 357

[3] Leroux B 2002 *PhD Thesis* Ecole Centrale Paris

[4] Lasheras JC, Villermaux E, Hopfinger EJ 1998 *Journal of Fluid Mechanics* **357** 28

[5] Juniper M 2001 *PhD Thesis* Ecole Centrale Paris

[6] Ishii M 1975 *Thermo-Fluid Dynamic Theory* Eyrolles, Paris

[7] Vallet A and Borghi R 1999 *C.R. Acad. Sci. Paris* **327** 1015

[8] Villermaux E 1998 *Journal of Propulsion and Power* **14** 807

[9] O'Rourke and Amsden A A 1987 *SAE Technical paper 972089*

[10] Werquin O 2001 *PhD Thesis* University of Rouen